Electronic Supplementary Material (ESI) for Energy & Environmental Science.
This journal is © The Royal Society of Chemistry 2024

Supporting Information

Customizing water-scarce, zinc ion-rich Helmholtz plane of zinc anode for Ah-scale Zn metal batteries

Guowei Gao,[a] Xiaomei Huo,[a] Boxin Li,[a] Jingxuan Bi,[a] Zhenkai Zhou,[a] Zhuzhu Du,[b] Wei Ai*[a] and Wei Huang*[a]

[a] Frontiers Science Center for Flexible Electronics and Xi'an Institute of Flexible Electronics, Northwestern Polytechnical University, Xi'an 710072, China. *E-mail: iamwai@nwpu.edu.cn, vc@nwpu.edu.cn

[b] School of Materials Science and Engineering & Institute of Flexible Electronics and Intelligent Textile, Xi'an Polytechnic University, Xi'an 710048, China

Experimental Section

Preparation of Zn@IL and Zn@IL&PPS: Zn@IL was synthesized by immersing Zn foil (100 μm) in a mixture of IL (99%) and deionized water. The foil was left in the solution for varying durations, then removed and heat-treated in a vacuum oven at 60 °C to evaporate the residual water. The synthesis procedure for Zn@IL&PPS followed a similar approach, with the Zn foil being immersed in a mixed solution of IL and PEDOT:PSS (1.5% in water) for different periods. Subsequently, the IL-doped hydrogel-coated Zn foil was dried in a vacuum oven at 60 °C to produce the Zn@IL&PPS.

Preparation of δ-MnO_2 cathode: 0.403 g of $MnSO_4$ and 2.529 g of $KMnO_4$ were dissolved in 70 mL of deionized water by stirring. The solution was then transferred into a reaction kettle and reacted at 160 °C for 12 h. The resulting precipitate was collected, thoroughly washed with deionized water and absolute ethanol to remove impurities, and then dried at 60 °C to obtain δ-MnO_2. The slurry, composed of 70 wt% δ-MnO_2 powders, 10 wt% polyvinylidene fluoride (PVDF) binder, and 20 wt% acetylene black, was blade-coated onto a carbon paper. It was then dried at 60 °C for 24 h to produce the δ-MnO_2 cathodes with a loading of ~4 mg cm^{-2}.

Preparation of I_2 cathode: The I_2 cathodes were prepared through electrodeposition.[1, 2] The working electrode, consisting of activated carbon (YP50F) and PVDF in a 1:1 ratio, was coated onto a stainless steel mesh with 200 mesh count. The typical mass loading of I_2 is 34.5 mg cm^{-2}.

Materials characterization: The morphologies and components of the samples were characterized using SEM (FEI Verios G4) with an energy dispersive spectrometry. The phases and structures were examined by XRD using a Bruker D8 instrument with Cu Kα radiation (λ = 0.154056 nm). FTIR of the samples were recorded with a Bruker Tensor 27. XPS was conducted on a Thermo Scientific K-Alpha instrument (Thermo Fisher Scientific). WAXS was conducted on a Xeuss 3.0 with a Cu Kα X-ray source. The optical images were taken by an optical microscope (Yueshi YM520R). The RTCs of different Zn lattice planes are calculated using the following formula:[3, 4]

$$RTC_{(hkl)} = \frac{I_{(hkl)}/I_{0(hkl)}}{\sum\left(I_{(hkl)}/I_{0(hkl)}\right)} * 100$$

where $I_{(hkl)}$ is the intensity obtained from experimental samples, and $I_{0(hkl)}$ is the intensity of the standard sample (PDF #04-0831).

Electrochemical measurements: For coin cell assembly, the Zn||Zn symmetrical cells, Zn||Cu asymmetric cells, and full cells were assembled using CR2032 coin cells. In symmetrical cell assembly, two Zn foils (ϕ = 12 mm) served as both the anode and cathode. In asymmetric cell assembly, a Zn foil (ϕ = 12 mm) anode was paired with a Cu foil cathode (10 μm, 99.99%, ϕ = 16 mm). For full cell assembly, a Zn foil (ϕ = 12 mm) anode was paired with a δ-MnO_2 cathode (ϕ = 12 mm). All cells were assembled in an open-air environment using Whatman GF/D as the separator, and each cell contained approximately 75 μL of 2 M $ZnSO_4$ electrolyte. For pouch cell assembly, δ-MnO_2 cathodes measured 5 cm × 5 cm and I_2 cathodes measured 10 cm × 10 cm. The electrolyte used was a mixed solution of 1 M $ZnSO_4$ and 0.1 M KI. Electrochemical tests were conducted on a NEWARE battery-testing system and an Autolab PGSTAT 302N electrochemical workstation. The frequency range for EIS spanned from 1 MHz to 1 Hz, while the voltage range for δ-MnO_2 and I_2-based cells was set at 0.8-1.8 V and 0.6-1.6 V, respectively. The transference numbers for Zn^{2+} (t_{Zn2+}) in the symmetrical Zn cells were evaluated using EIS before and after the CA test,[5, 6] calculated as follows:

$$t_{Zn^{2+}} = \frac{I_S\left(\Delta V - I_O R_O\right)}{I_O\left(\Delta V - I_S R_S\right)}$$

where ΔV represents the applied voltage polarization (25 mV), I_S and R_S are the steady state current and resistance, respectively, and I_0 and R_0 are the initial current and resistance, respectively.

Computational detail: DFT calculations were performed to investigate adsorption energy between the Zn (002) and various ions using the CASTEP method.[1] The calculations employed the Generalized Gradient Approximation with the Perdew-Burke-Ernzerhof formulation, providing an accurate representation of the exchange-correlation energy.[7-10] A cutoff energy of 550 eV was selected for the plane-wave basis,

and ultrasoft pseudopotentials were used. Geometry optimizations were conducted using the Broyden-Fletcher-Goldfarb-Shannon algorithm.[11] The Zn (002) slab, characterized by lattice parameters a = b = 14.2339 Å and c = 21.4328 Å with angles α = β = 90° and γ = 120°, consists of four layers; the bottom two layers were fixed while the others were allowed to relax during optimizations. The slab models were constructed using the standard crystallographic information file for the Zn primitive cell, ensuring a minimum vacuum thickness of 15 Å to prevent interactions between slabs. For all energy minimizations, a k-point grid of 3 × 3 × 1 was employed. The convergence criteria for the geometry optimizations were set such that the Hellmann-Feynman forces on any atom should not exceed 0.03 eV $Å^{-1}$, and the total energy difference and the inter-ionic displacement should be less than 1×10^{-5} eV/atom and 0.001 Å/atom, respectively. The adsorption energy (ΔE_{ads}) was calculated as follows:

$$\Delta E_{ads} = E*_{ads} - E_{ads}$$

where E_{*ads} is the total energy of the slab model and the ion, and E_{ads} is the energy of the isolated Zn atom.

Finite element method simulations: The distribution of electrolyte potential and current density during Zn electrodeposition was investigated using COMSOL Multiphysics software, which utilizes the finite element method. For this analysis, the Zn array on the surface of the Zn electrode was modeled as semi-elliptical cones. The boundary conditions applied to the electrodes were governed by the Butler-Volmer equation.[12] The voltage difference across the electrodes was established at 0.1 V (vs. Zn/Zn^{2+}), with an initial Zn^{2+} ions concentration set at 2 M. The diffusion coefficient of Zn^{2+} ions within the electrolyte was set to 1×10^{-9} m^2 s^{-1}. The average current density across the cell was set as 25 A m^{-2}.

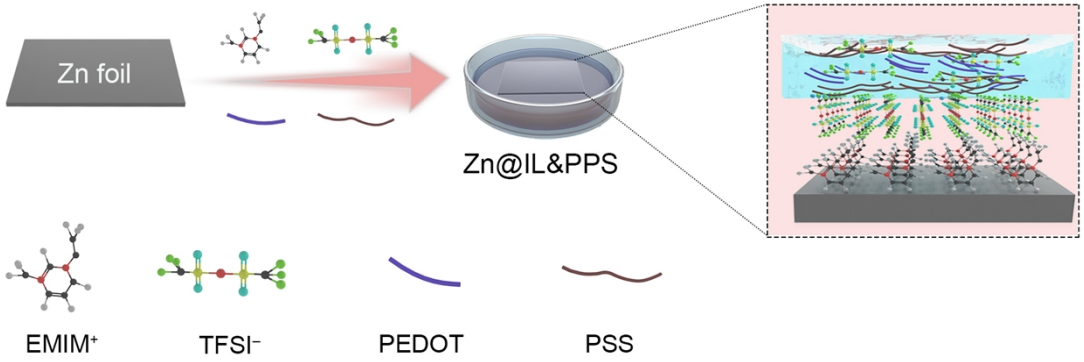

Fig. S1 Schematic diagram of the synthesis of Zn@IL&PPS.

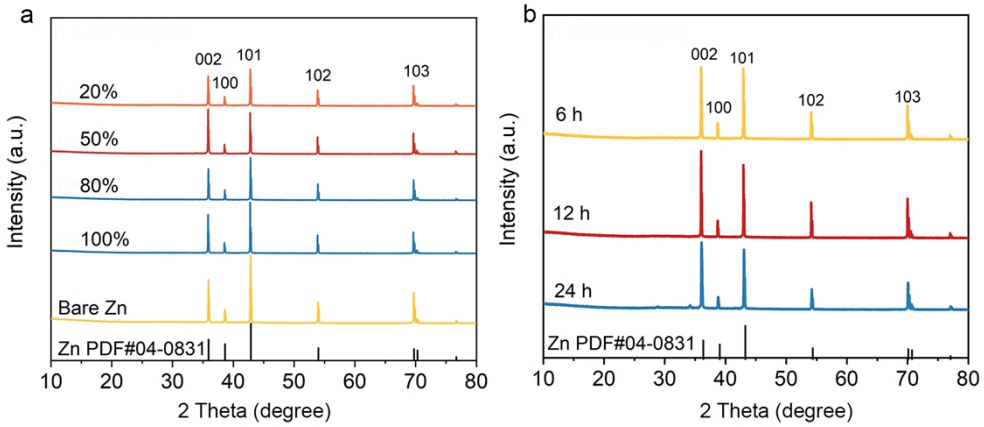

Fig. S2 (a) XRD patterns of the Zn foils treated by IL and PEDOT:PSS at varying volume ratios. (b) XRD patterns of the Zn foils treated by 1:1 of IL and PEDOT:PSS at different times.

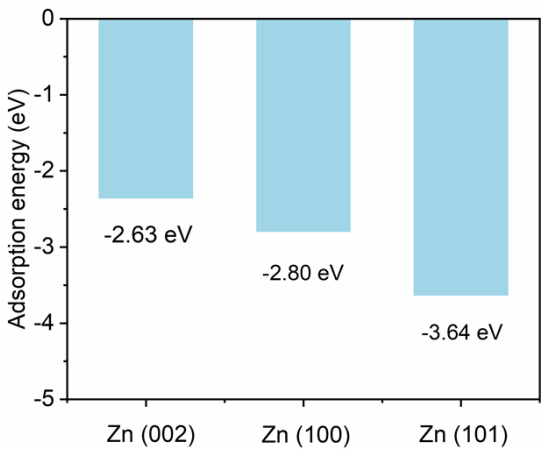

Fig. S3 DFT calculated absorption energy of $EMIM^+$ on different facets of Zn.

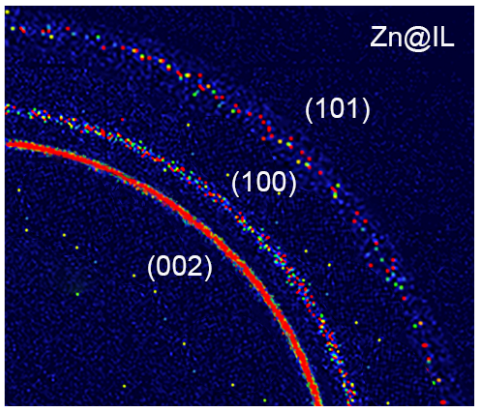

Fig. S4 2D WAXS patterns of Zn@IL.

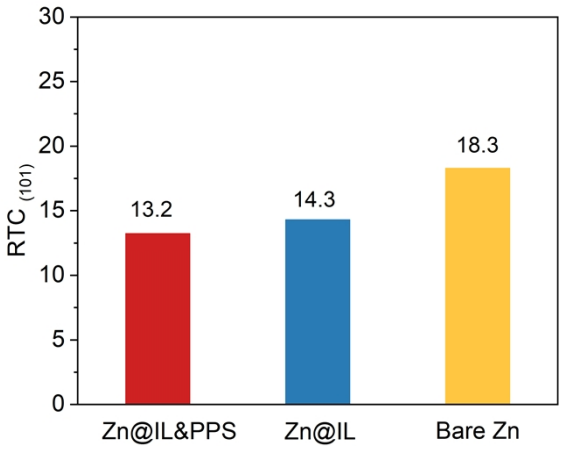

Fig. S5 $RTC_{(101)}$ of the bare Zn, Zn@IL and Zn@IL&PPS.

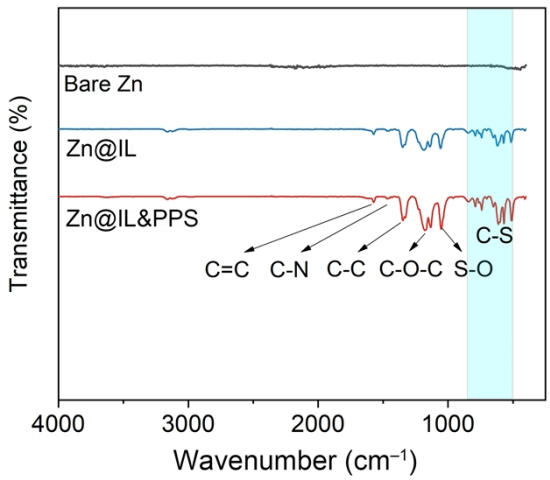

Fig. S6 FTIR spectra of the bare Zn, Zn@IL, and Zn@IL&PPS.

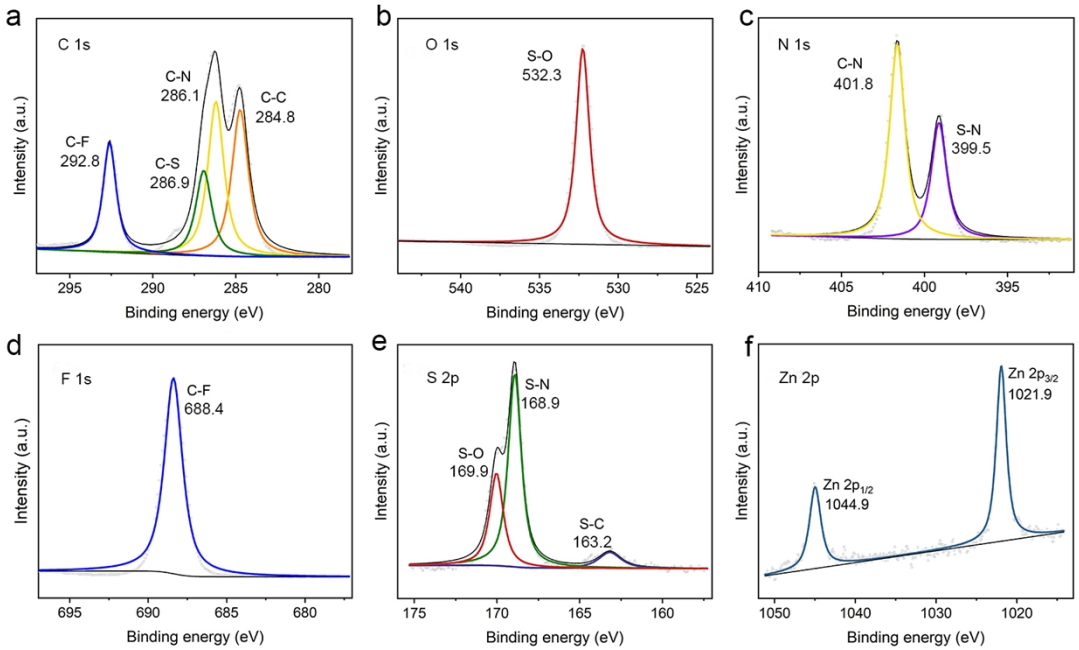

Fig. S7 The C 1s, O 1s, N 1s, F 1s, S 2p, Zn 2p XPS spectra of Zn@IL.

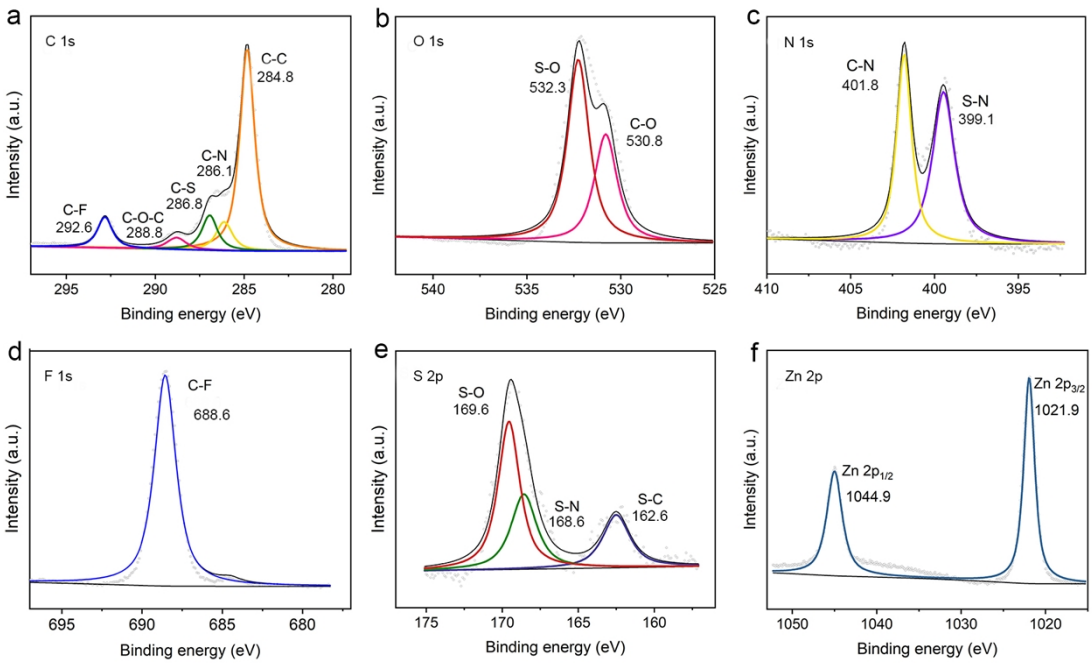

Fig. S8 The C 1s, O 1s, N 1s, F 1s, S 2p, Zn 2p XPS spectra of Zn@IL&PPS.

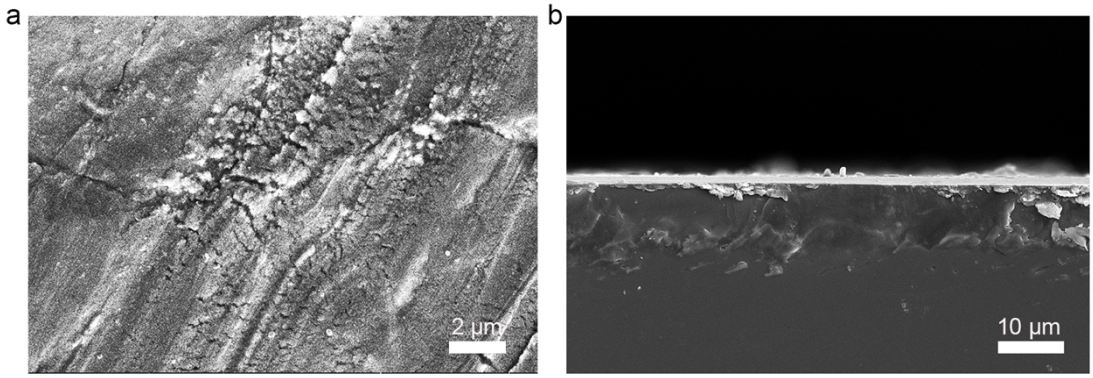

Fig. S9 (a) Top-view and (b) cross-sectional SEM images of bare Zn.

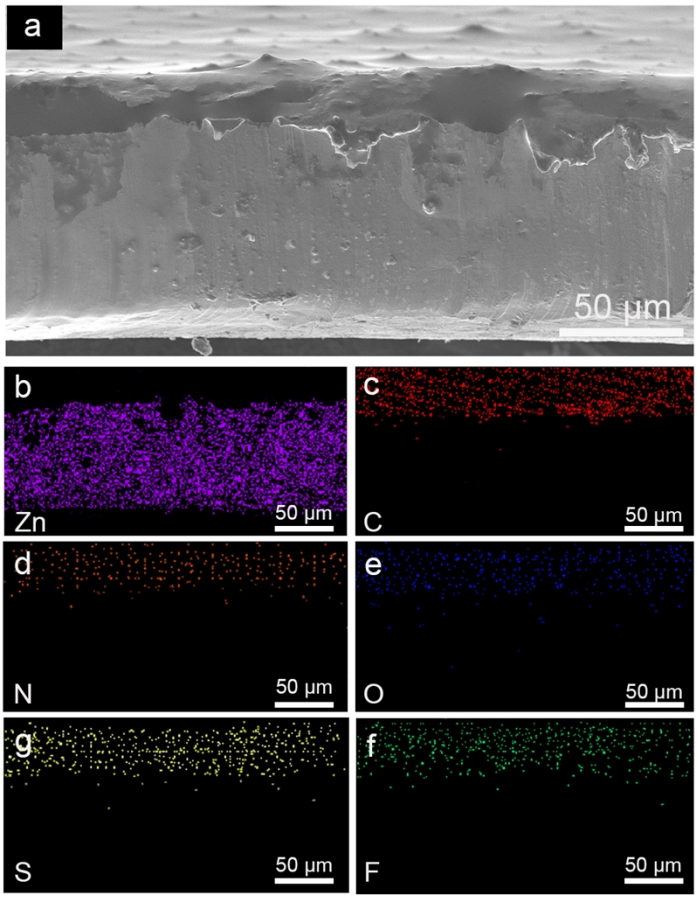

Fig. S10 SEM and the corresponding EDS mapping images of Zn@IL&PPS.

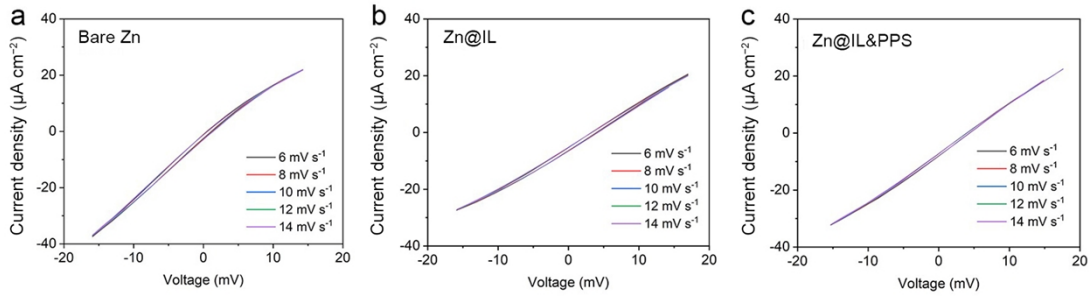

Fig. S11 CV curves of the Zn symmetric cells.

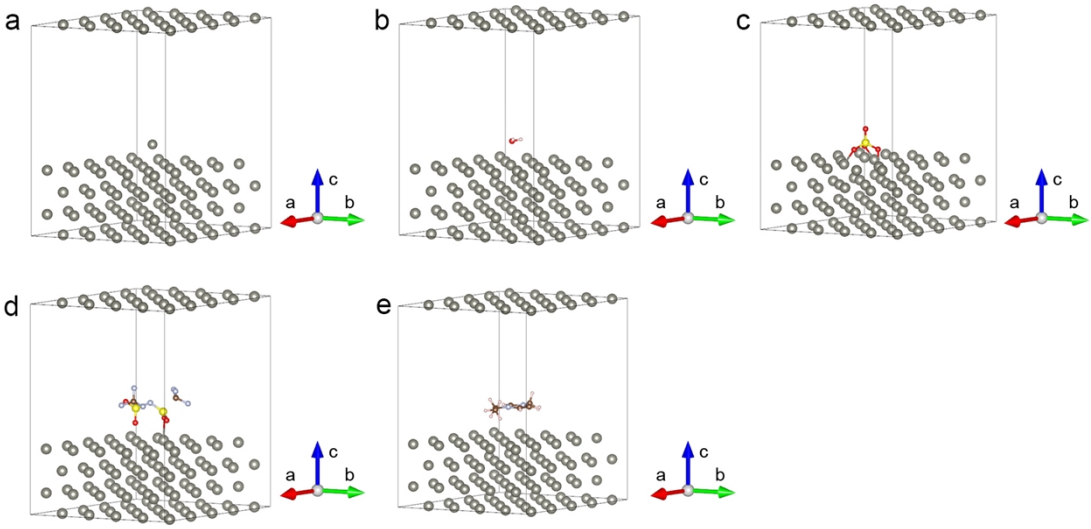

Fig. S12 Different adsorption models between (a) Zn, (b) H_2O, (c) SO_4^{2-}, (d) $TFSI^-$, (e) $EMIM^+$ and Zn (002) plane.

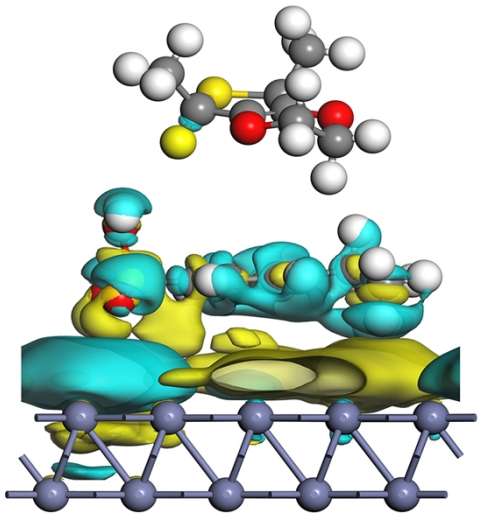

Fig. S13 Top view of the CDD of $EMIM^+$ on Zn (002) plane.

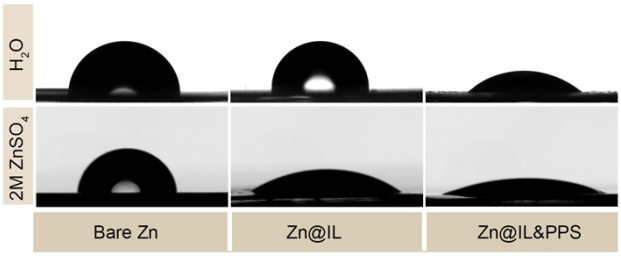

Fig. S14 Optical images showing the contact angles of various Zn foils.

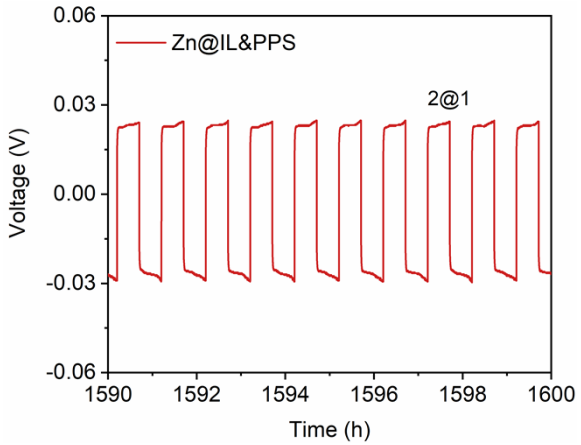

Fig. S15 The enlarged voltage curves of Zn@IL&PPS electrode at 2@1.

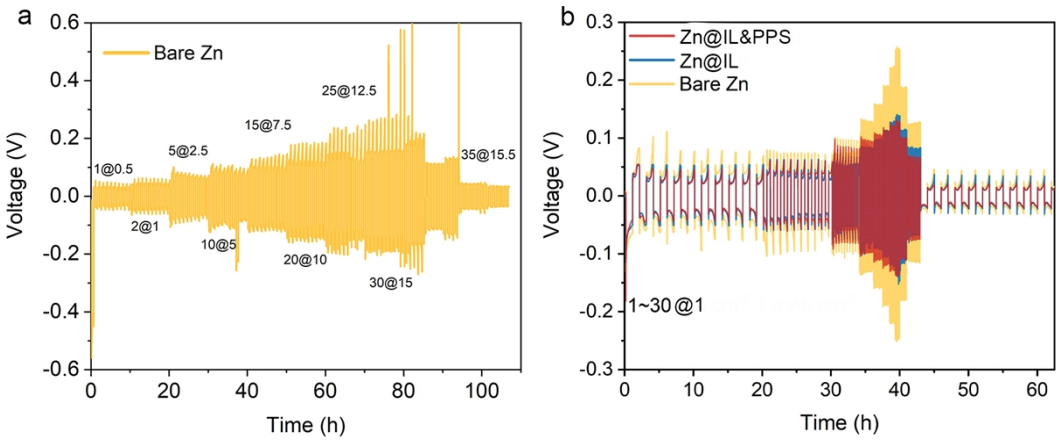

Fig. S16 Rate testing of (a) bare Zn symmetric cell and (b) different Zn electrodes.

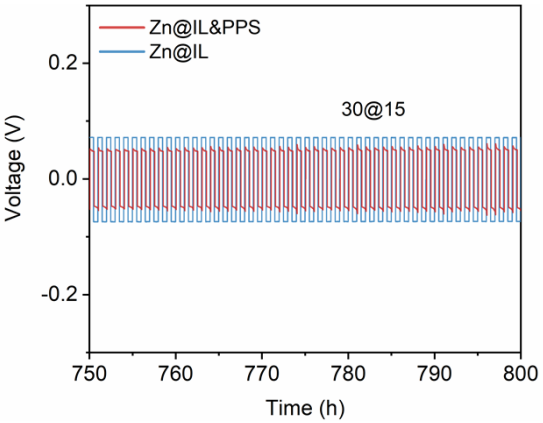

Fig. S17 The enlarged voltage curves of different electrodes at 30@15.

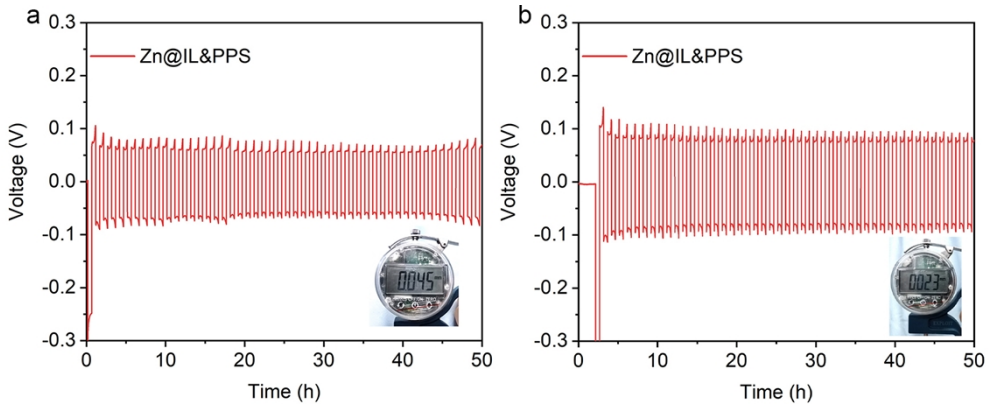

Fig. S18 Galvanostatic cycling performance of the Zn@IL&PPS symmetrical batteries with electrode thickness of (a) 45 and (b) 23 μm depth of discharge of about 25%.

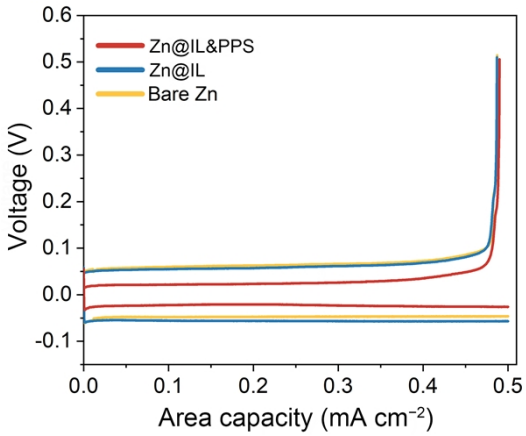

Fig. S19 Voltage profiles of the Zn||Cu asymmetric cells at 1@0.5.

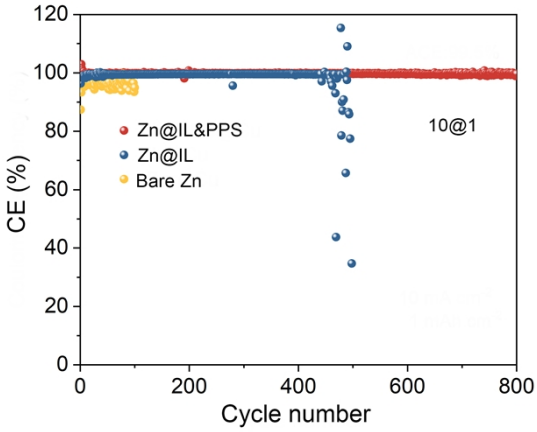

Fig. S20 CE of the Zn||Cu asymmetric cells at 10@1.

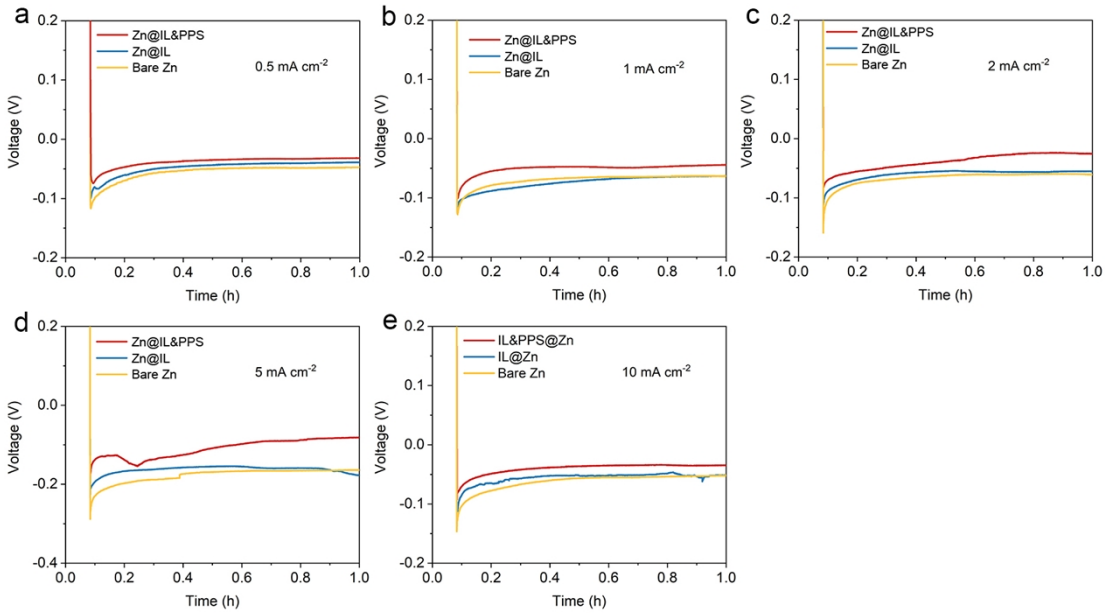

Fig. S21 Nucleation overpotential of Zn||Cu asymmetric cells at different current densities.

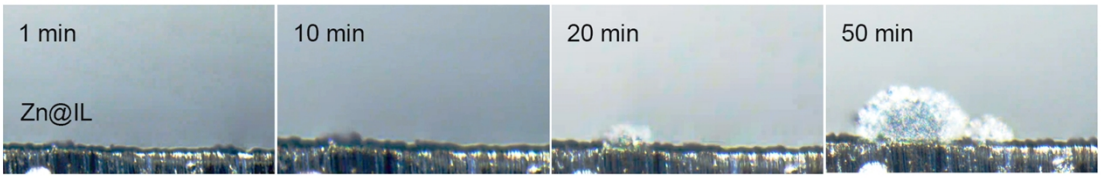

Fig. S22 In situ optical microscopy images of Zn deposition on Zn@IL.

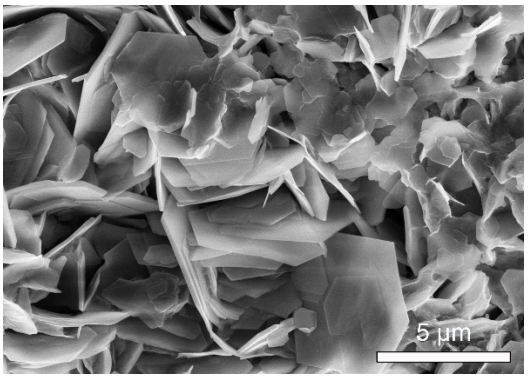

Fig. S23 SEM image of the cycled Zn@IL.

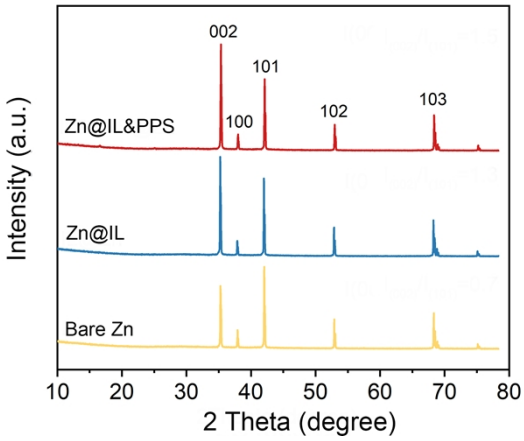

Fig. S24 XRD patterns of the cycled Zn electrodes.

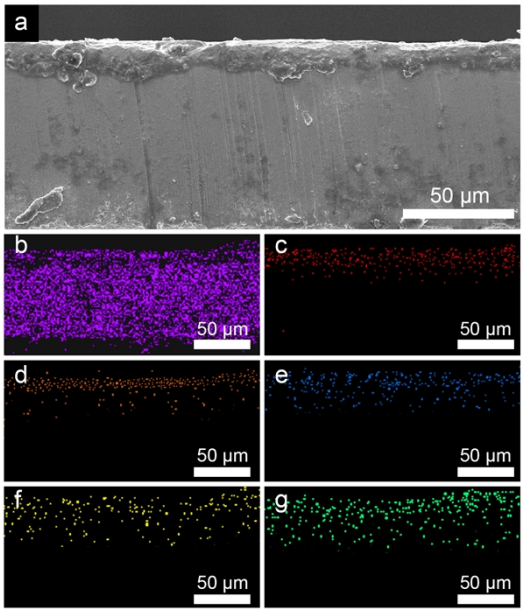

Fig. S25 SEM and the corresponding EDS mapping images of the cycled Zn@IL&PPS.

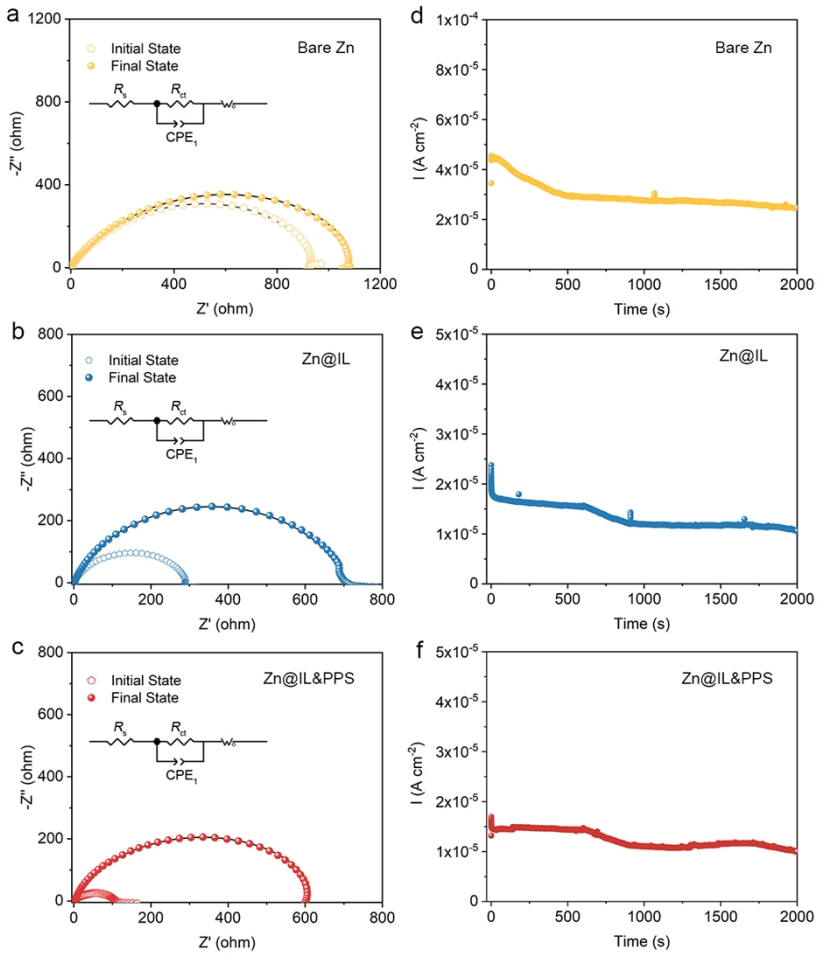

Fig. S26 Nyquist plots of (a) bare Zn, (b) Zn@IL, and (c) Zn@IL&PPS electrodes before and after CA measurement. Inset: the equivalent circuit model of EIS. The CA curves of (d) bare Zn, (e) Zn@IL, and (f) Zn@IL&PPS electrodes.

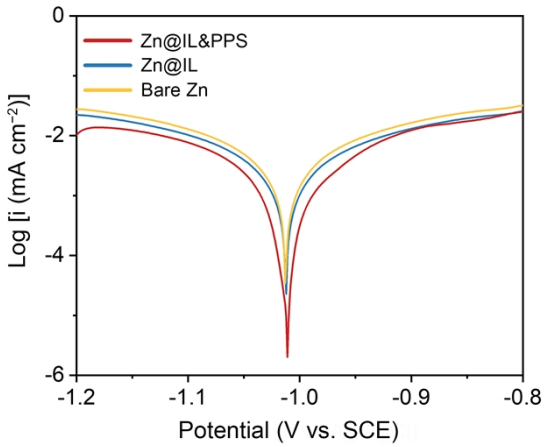

Fig. S27 Tafel plots of different Zn electrodes.

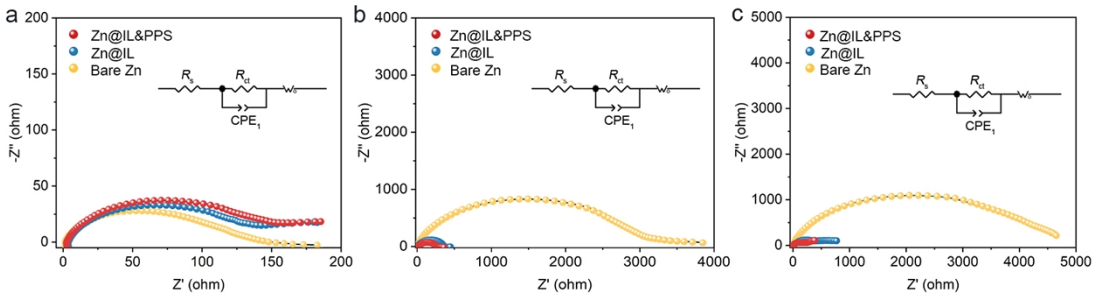

Fig. S28 Nyquist plots of Zn electrodes (a) before, and after soaking in $ZnSO_4$ electrolytes for (b) 12 and (c) 24 h. Inset: the equivalent circuit model of EIS.

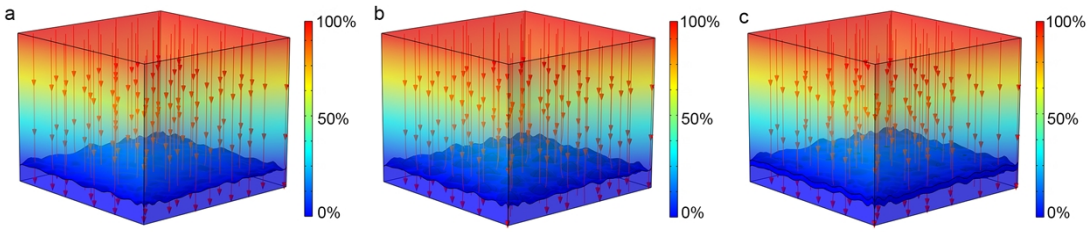

Fig. S29 Simulations of the surface potential of (a) bare Zn, (b) Zn@IL, and (c) Zn@IL&PPS.

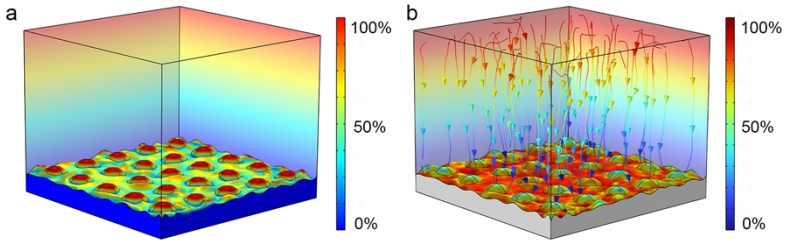

Fig. S30 Simulations of the (a) electric field and (b) Zn^{2+} concentration field distribution on the surface of Zn@IL.

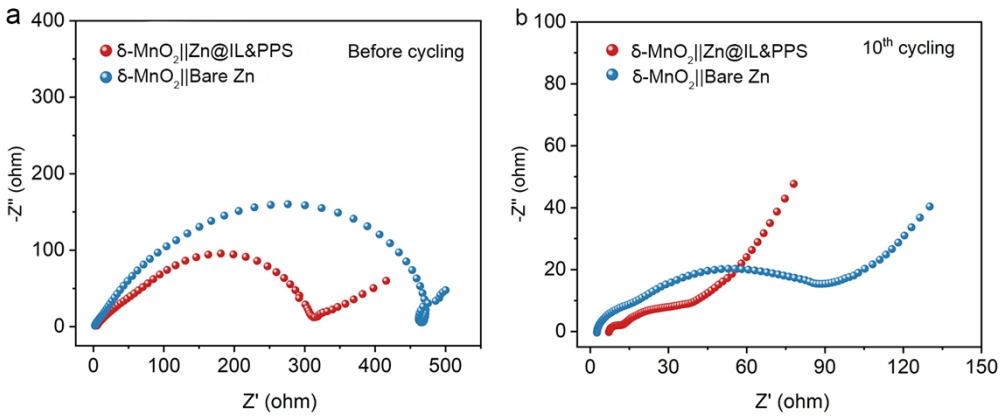

Fig. S31 Nyquist plots of the δ-MnO_2||Zn and δ-MnO_2||Zn@IL&PPS batteries (a) before and (b) after 10 cycles.

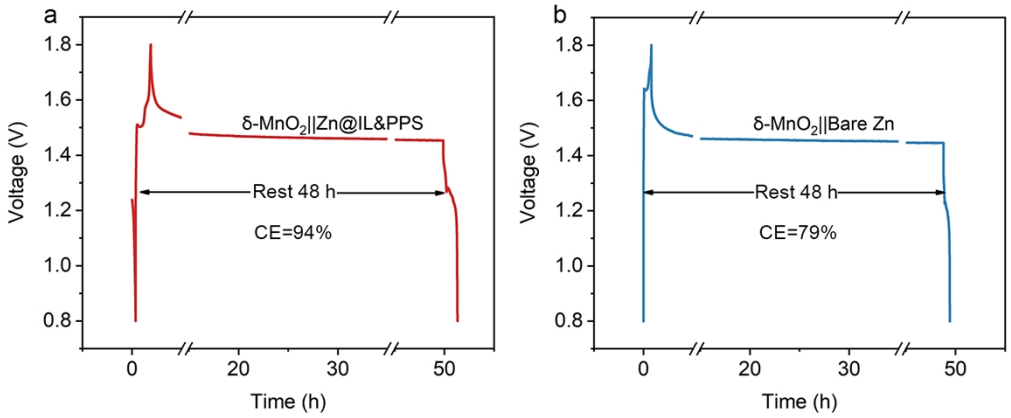

Fig. S32 Self-discharge testing of the δ-MnO_2||Zn@IL&PPS and δ-MnO_2||bare Zn batteries.

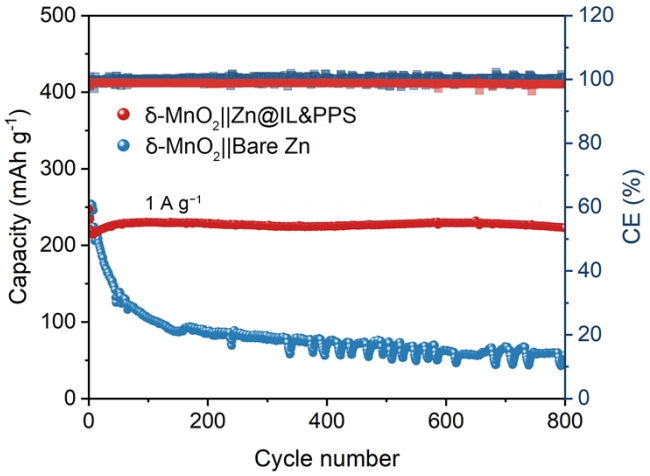

Fig. S33 Cycling performance of the coin cells at 1 A g^{-1}.

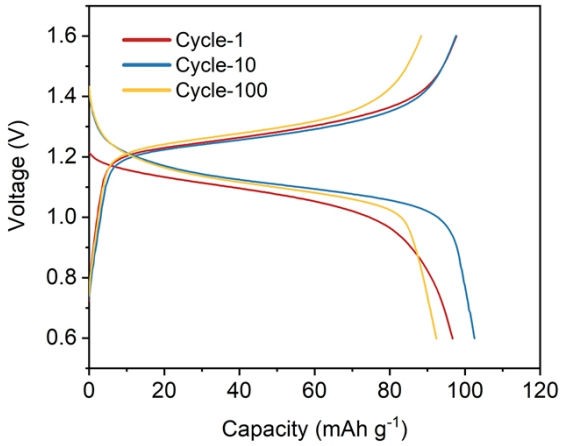

Fig. S34 Charge/discharge curves of the I_2||Zn@IL&PPS pouch cell.

Table S1. The atomic ratio of Zn@IL&PPS and Zn@IL.

Sample	C	F	N	O	S	Zn
Zn@IL&PPS	47.88	15.53	7.67	22.52	5.89	0.51
Zn@IL	38.01	26.85	11.4	11.92	7.3	4.52

Table S2. Summary of the contact angles of bare Zn, Zn@IL, and Zn@IL&PPS.

Samples	H_2O	2 M $ZnSO_4$
Bare Zn	83.9	80.3
Zn@IL	87.3	37.9
Zn@IL&PPS	43.7	21.2

Table S3. Comparison of the electrochemical performance of Zn||Zn symmetric cells.

Modifications	Current density (mA cm^{-2})	Capacity (mAh cm^{-2})	Cycling (h)	Ref
HP-Zn	2	1	1400	Adv. Energy Mater. 2023, 13, 2300932
TFA-AN@Zn	4	2	1000	Adv. Energy Mater. 2022, 12, 2102797
$Zn(TCNQ)_2$	5	5	220	ACS Energy Lett. 2023, 8, 2718
COP/Cu@Zn	4	4	500	Adv. Funct. Mater. 2023, 33, 2302293
NGO@Zn	5	5	300	Adv. Mater. 2021, 33, 2101649
Etched Zn	20	10	400	Energy Environ. Sci. 2024, 17, 642
Zn(002)@ZPO	20	10	500	ACS Nano 2023, 17, 15113
PM@Zn	20	1	400	Angew. Chem. Int. Ed. 2023, 62, 2304454
$Zn@ZnF_2$	1	1	800	Adv. Mater. 2021, 33, 2007388
Modified Zn	10	10	500	Energy Environ. Sci. 2023, 16, 275
Zn@IL&PPS	**2**	**1**	**1600**	**This work**
	30	**15**	**800**	

Table S4. Comparison of the electrochemical performance of I_2||Zn batteries.

Sample	Mass loading (mg cm^{-2})	Capacity (mAh cm^{-2})	Energy density (Wh kg^{-1})	Current density (mA cm^{-2})	Electrolyte	Ref
Zn@PFPA	9	1.17	143	18	2 M $ZnSO_4$	13
Zn-BTC	2	0.2	110	3.8	0.5 M $ZnSO_4$, 1 M LiI and 0.1 M I_2	14
SC-PPS@Zn	2	0.17	102	6.4	2 M $ZnSO_4$	15
Starch/I_2/Zn	3	0.27	75	6	0.5 M $ZnSO_4$, 1 M LiI and 0.1 M I_2	16
PDMS/TiO_{2-x}	1.5	1	192	1	1 M or 3 M $ZnSO_4$	17
Pyridine-$ZnSO_4$	3.2	0.57	198	0.6	pyridine-$ZnSO_4$	18
PVDF-Sn@Zn	0.8	5	240	5	2 M $ZnSO_4$	19
B-Fe-NC/I_2	3.5	0.16	225	0.7	2 M $ZnSO_4$	20
BR-Zn	20	1.1	55	10	2 M $ZnSO_4$	21
Zn@IL&PPS	**37.5**	**6.25**	**239**	**7.5**	**1 M $ZnSO_4$ and 0.1 M KI**	**This work**

References

[1] C. Prehal, H. Fitzek, G. Kothleitner, V. Presser, B. Gollas, S. A. Freunberger and Q. Abbas, *Nat. Commun.*, 2020, **11**, 4838.

[2] X. Jin, L. Song, C. Dai, Y. Xiao, Y. Han, X. Li, Y. Wang, J. Zhang, Y. Zhao, Z. Zhang, N. Chen, L. Jiang and L. Qu, *Adv. Mater.*, 2022, **34**, 2109450.

[3] M. Zhou, S. Guo, J. Li, X. Luo, Z. Liu, T. Zhang, X. Cao, M. Long, B. Lu, A. Pan, G. Fang, J. Zhou and S. Liang, *Adv. Mater.*, 2021, **33**, 2100187.

[4] Q. Zhao, T. Xu, K. Liu, H. Du, M. Zhang, Y. Wang, L. Yang, H. Zhang, X. Wang and C. Si, *Energy Storage Mater.*, 2024, **71**, 103605.

[5] L. Suo, Y.-S. Hu, H. Li, M. Armand and L. Chen, *Nat. Commun.*, 2013, **4**, 1481.

[6] Z. Zhao, J. Zhao, Z. Hu, J. Li, J. Li, Y. Zhang, C. Wang and G. Cui, *Energy Environ. Sci.*, 2019, **12**, 1938-1949.

[7] S. J. Clark, M. D. Segall, C. J. Pickard, P. J. Hasnip, M. I. J. Probert, K. Refson, M. C. Payne, Z. *Kristallogr.*, 2005, **220**, 567-570.

[8] P. J. Hasnip, C. J. Pickard, Comput. *Phys. Commun.*, 2006, **174**, 24-29.

[9] J. P. Perdew, K. Burke, M. Ernzerhof, *Phys. Rev. Lett.*, 1996, **77**, 3865.

[10] J. P. Perdew, J. A. Chevary, S. H. Vosko, K. A. Jackson, M. R. Pederson, D. J. Singh, C. Fiolhais, *Phys. Rev. B*, 1992, **46**, 6671.

[11] J. D. Head, M. C. Zerner, *Chem. Phys. Lett.*, 1985, **122**, 264-270.

[12] P. Wang, S. Liang, C. Chen, X. Xie, J. Chen, Z. Liu, Y. Tang, B. Lu, J. Zhou, *Adv. Mater.*, 2022, **34**, 2202733.

[13] S. Huang, R. Tang, X. Liu, Y. Zhang, Y. Tang, Z. Wen, M. Ye, Y. Yang, C. C. Li, *Energy Environ. Sci.*, 2024, **17**, 591-601.

[14] H. Yang, Y. Qiao, Z. Chang, H. Deng, P. He, H. Zhou, *Adv. Mater.*, 2020, **32**, 2004240.

[15] L. Zhang, J. Huang, H. Guo, L. Ge, Z. Tian, M. Zhang, J. Wang, G. He, T. Liu, J. Hofkens, D. J. L. Brett, F. Lai, *Adv. Energy Mater.*, 2023, **13**, 2203790.

[16] S.-J. Zhang, J. Hao, H. Li, P.-F. Zhang, Z.-W. Yin, Y.-Y. Li, B. Zhang, Z. Lin, S.-Z. Qiao, *Adv. Mater.*, 2022, **34**, 2201716.

[17] Z. Guo, L. Fan, C. Zhao, A. Chen, N. Liu, Y. Zhang, N. Zhang, *Adv. Mater.*, 2022,

34, 2105133.

[18] Y. Lyu, J. A. Yuwono, P. Wang, Y. Wang, F. Yang, S. Liu, S. Zhang, B. Wang, K. Davey, J. Mao, Z. Guo, *Angew. Chem. Int. Ed.*, 2023, **62**, 202303011.

[19] Q. Cao, Y. Gao, J. Pu, X. Zhao, Y. Wang, J. Chen, C. Guan, *Nat. Commun.*, 2023, **14**, 641.

[20] M. Liu, Q. Chen, X. Cao, D. Tan, J. Ma, J. Zhang, *J. Am. Chem. Soc.*, 2022, **144**, 21683.

[21] Z. Yang, C. Hu, Q. Zhang, T. Wu, C. Xie, H. Wang, Y. Tang, X. Ji, H. Wang, *Angew. Chem. Int. Ed.*, 2023, **62**, 202308017.